International Journal on Advanced Science Engineering Information Technology

Vol.13 (2023) No. 1
ISSN: 2088-5334

Simulation of Single-Phase on-Grid Photovoltaic Inverter for Power Injection and Active Power Filter

Susatyo Handoko [a,*], Mochammad Facta [a], Tejo Sukmadi [a]

[a] *Electrical Engineering Department, Faculty of Engineering, Diponegoro University, Semarang, 50275, Indonesia*
Corresponding author: [*]susatyo@elektro.undip.ac.id

***Abstract*— Currently, most photovoltaic (PV) sources are connected to the grid. This research discusses single-phase on-grid PV inverters. A two-stage inverter which consisted of a boost-type DC-DC converter and a single-phase inverter, was used. In addition, the inverter improved the power quality to deliver PV maximum power. The entire power generated by PV was to be delivered to PCC, and power quality in PCC was also improved. In this system, the grid only drew or supplied active power. The P&O algorithm, as a simple algorithm, was used to control the boost converter to obtain the maximum PV power. In a single-phase inverter, the DC link voltage regulation was carried out using the PI control (outer loop), while the hysteresis control was used to control the output current (inner loop). The voltage control regulated the power delivered from the PV to the PCC by maintaining a constant DC bus voltage at the specified value. With the current control, a single-phase inverter provided two compensations: reactive power and harmonics. In this research, a simulation to control a two-stage inverter was created by using PSIM. Irradiation for PV was varied between 0-1000 W/m^2 for 5 seconds. The simulation results showed that the controls performed could work well, as shown by the maximum power injection from the PV to the PCC in which the grid current was sinusoidal (harmonic mitigation) and reactive power compensation was performed.**

***Keywords*—Photovoltaic; inverter; single phase; active power filter; power quality.**

Manuscript received 16 Nov. 2021; revised 30 May 2022; accepted 18 Sep. 2022. Date of publication 28 Feb. 2023.

I. INTRODUCTION

Today, there is an increase in electric power demand in the world. However, the energy obtained from conventional sources is also accompanied by environmental pollution; consequently, the availability of conventional energy sources at this time needs serious attention [1]. Therefore, the need for the use of renewable energy sources in the future comes to be a consideration. Various promising renewable energy sources include photovoltaic, wind, and geothermal. Here, photovoltaic energy can offer numerous advantages, such as abundant availability, cleanness, and cost-free, that need to be considered [2].

Various installed loads can be the factors of power quality issues, such as power factor and harmonics in the power system. Harmonic compensation in the power system can be done by using an Active Power Filter (APF). The development of power electronics greatly affected the performance of active power filters in compensating harmonics [3]. With the advancement of digital control and power electronics technology, distributed generators can also be used to improve power quality. On-grid inverter control can be done so that the current injected by the grid has minimum harmonics [4]. Several control methods for reducing harmonics in PCC have been discussed using: Synchronous Reference Frame theory [5], fuzzy [6], [7], adaptive noise cancellation [8], sliding mode control [9], Lyapunov approach [10], direct power control with space vector modulation strategy (DPC-SVM) [11], hybrid automaton control [12], and virtual impedance [13], [14].

The connection of most DG units to the utility is done using power electronics-based equipment that will control the operation of the DG units. Single-phase on-grid inverters are widely used in renewable energy applications, for example, in PV systems. In many kinds of literature, there have been many discussions about control methods for grid-connected inverters; some of them are predictive control [15], hysteresis control [16], adaptive hysteresis control [17], adaptive integrator using AMN [18], and PQ theory control [19]. Hysteresis can be used to control the inverter current by using a certain bandwidth. In conventional hysteresis control, constant bandwidth is used, while in adaptive hysteresis control, variable bandwidth is used. Adaptive hysteresis band

current control used in active power filters for photovoltaics was discussed in [17]. DC bus voltage regulation on the outer loop could be done using proportional-integral (PI) control. Adaptive integrators are used in on-grid inverters when the grid voltage is unbalanced [18]. Comparison of single-phase shunts active power filter (SAPF) using PQ and SRF theories [19]. These control strategies have been used in various inverter applications, both off-grid and on-grid. In the on-grid case, the inverter is used not only for power injection but also for power quality improvement [20]–[23].

In this paper, simulation and analysis were carried out on a grid-connected inverter for PV application. Single-phase PV inverter was controlled for maximum power injection and active power filter (APF). The active power filter provided reactive power compensation and harmonic mitigation. Simulations were carried out using PSIM, and several irradiation variations were carried out for the analysis.

II. Material and Method

A. System configuration

Fig. 1 illustrates the schematic of the system discussed. The system has five main components: single-phase source, solar array (PV), boost converter, single-phase inverter, and load. In addition, it included two control components, namely control for the boost converter and the single-phase inverter.

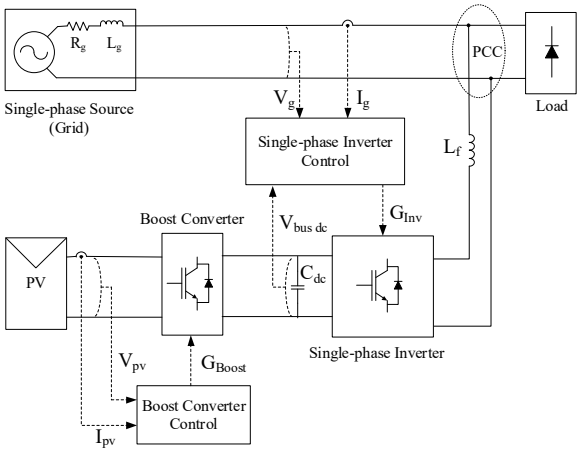

Fig. 1 Schematic of the system

1) Single-phase source (grid): The single-phase source used consisted of a voltage source and a grid impedance with resistance (R_g) = 0.1 Ω and inductance (L_g) = 1µH. The RMS voltage was 220 volts with a frequency of 50 Hz.

2) Solar Array (PV): The specifications of the PV module used in the study is presented in Table 1. The PV modules used for analysis were 50 (10 series and 5 parallel).

TABLE I
THE SPECIFICATIONS OF PV MODULE AT STC

Specification	Symbol	Value
Maximum power	P_{MAX}	250 Wp
Open circuit voltage	V_{OC}	37.8 V
Short circuit current	I_{SC}	8.28 A
Maximum power voltage	V_{MPP}	31.1 V
Maximum power current	I_{MPP}	8.05 A

*STC : 1000 W/m², 25ºC, AM 1.5

3) Boost converter: This research used a boost-type DC-DC converter. It is a circuit that converts a DC voltage into a larger DC voltage. Fig. 2 shows the boost converter circuit used in this study.

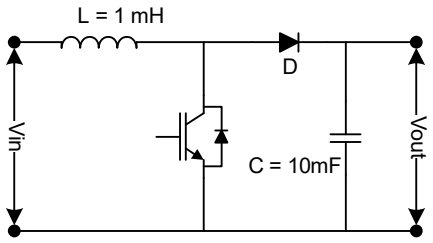

Fig. 2 Boost converter circuit

4) Single-phase inverter: This research used a single-phase bridge inverter to convert DC voltage into AC voltage. Fig. 3 shows a circuit of a single-phase DC-AC inverter.

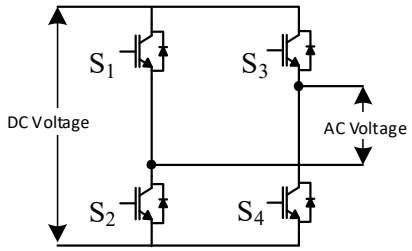

Fig. 3 Single-phase DC-AC inverter

5) Load: The load used in this research consisted of 3 components: rectifier, inductance, and resistance. Fig. 4 shows a circuit of the load.

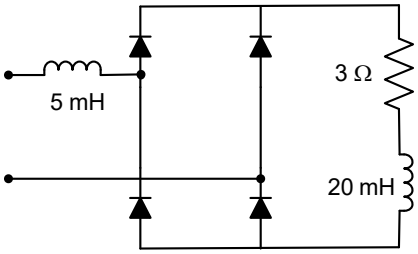

Fig. 4 Load

B. Control strategy

This section discusses the controls for boost converters and single-phase inverters.

1) Boost converter Control: The Perturb & observe (P&O) algorithm was used to control the boost converter. This algorithm is used for tracking the maximum power point. Fig. 5 shows the Perturb & Observe (P&O) flow chart. The inputs for P&O algorithm were voltages and currents of PV for t (new) and t-Δt (prev). In this algorithm, perturbation is provided to the PV module. The PV voltage is increased or decreased to check whether the output power increases or decreases. The P&O algorithm would produce a reference voltage as output that was obtained after the process of increasing and decreasing the voltage. Compared to the actual PV voltage, the reference voltage resulted in a voltage error. Based on the error, the gate signal for the boost converter would be generated using a hysteresis controller.

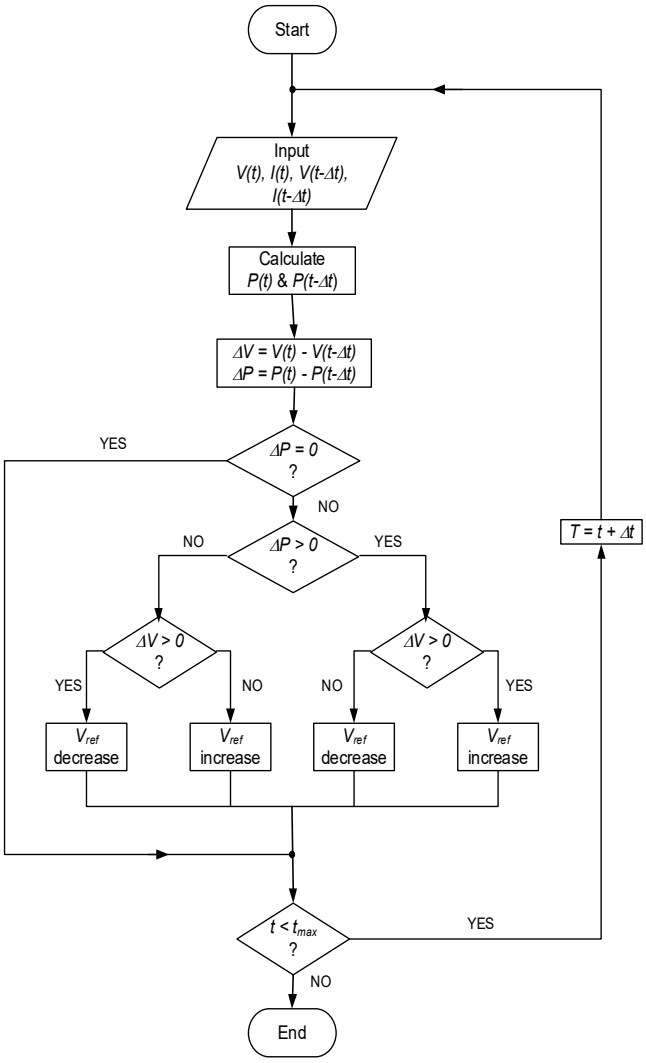

Fig. 5 Perturb and Observe (P&O) algorithm

2) Single Phase Inverter Control: Fig. 6 shows the block diagram of on-grid inverter control. There are four important components for this inverter control, i.e., DC voltage regulator, PLL, current calculation, and current controller.

The DC bus voltage was kept constant to determine the power delivered from PV to PCC. A DC voltage regulator carried out DC bus voltage regulation. Meanwhile, the function of a phase-locked loop (PLL) was to find the phase angle of the voltage. This angle was used to adjust the phase angle of the grid current. Then, the peak current generated by the grid was calculated by the Reference Current Calculation block. Once the peak current and phase angle have been known, the grid reference current could be determined. The switching pulse for the gate drives was generated by the hysteresis current controller based on that reference current.

With the control described above, the inverter would have a dual function: inject power and improve power quality. Power quality improvements carried out at PCC included reactive power compensation and mitigation in grid current harmonics. The filter inductance (L_f) was installed between the inverter and the PCC.

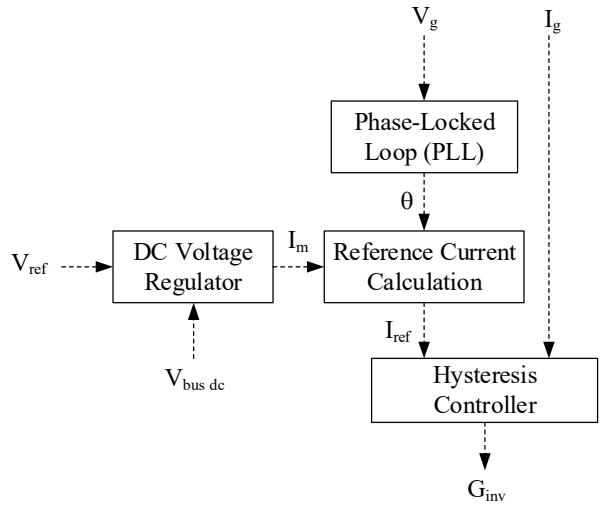

Fig. 6 Block diagram of single-phase inverter control

3) DC voltage regulator: The function of this regulator is to maintain the DC bus voltage remain constant. Through this regulation, the power flow in the system can be adjusted. There is a proportional integral controller inside this regulator. The input of this regulator is the dc bus voltage error. It is obtained by calculating the difference between the reference and DC bus voltage. The dc-link voltage error was obtained by:

$$V_{err} = V_{ref} - V_{dc} \tag{1}$$

The output is the reference current (I_m) for the grid current. Phase-locked loop (PLL) synchronizes I_m with the grid voltage. Fig. 7 shows the block diagram of this regulator.

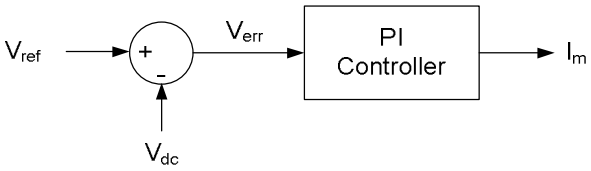

Fig. 7 Block diagram of DC voltage regulator

4) Phase-Locked Loop: Phase-locked loop (PLL) can be used to determine the phase and frequency of the electrical systems. In this study, the reference current was synchronized with the grid voltage using this PLL. Fig. 8 shows the basic configuration of the PLL using in this study.

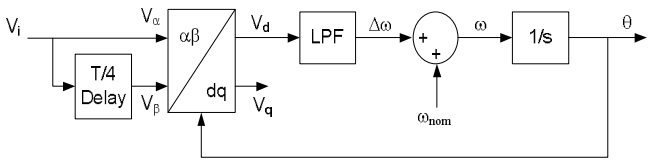

Fig. 8 Configuration of the PLL used in this study

5) Reference Current Calculation: This block combined the output of DC voltage regulator and PLL. The result obtained was the reference current for the grid current, which has already been synchronized with the grid voltage. The current was then computed as

$$I_{ref} = I_{m(LPF)}.\sin(\theta) \tag{2}$$

Fig. 9 shows the schematic for this calculation.

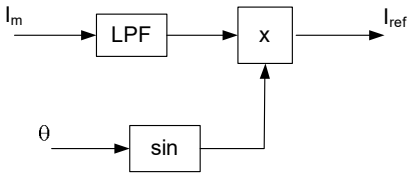

Fig. 9 Reference current calculation

6) Hysteresis Controller: The switching pulse on the inverter is generated by this controller. The difference between the reference and actual current is calculated, then compared with the hysteresis bandwidth. The IGBT switching pattern for the inverter in Fig. 3 is explained as follows:

If (Iref - I) > +hb, then the switch of S1 and S4 will be ON and the switch of S2 and S3 will be OFF.

If (Iref - I) < -hb, then the switch of S2 and S3 will be OFF and switch of S1 and S4 will be ON.

where hb is the width of hysteresis band.

III. Result and Discussion

Simulations studies were carried out to prove the performance of the control method. The system parameters are given in Table 2.

TABLE II
SYSTEM PARAMETERS

Parameter	Value
RMS Source Voltage (1-phase)	V_g = 220 V; f = 50 Hz
Source Impedance	R_g = 0.1 Ω; L_g = 1 µH
DC Bus Voltage	V_{ref} = 400V
Filter Inductance	L_f = 3 mH

The simulation block using PSIM for the system under study is shown in Fig. 10. The inverter has two functions, i.e., as a converter to inject power and an active power filter. It works to inject maximum power generated by PV to PCC.

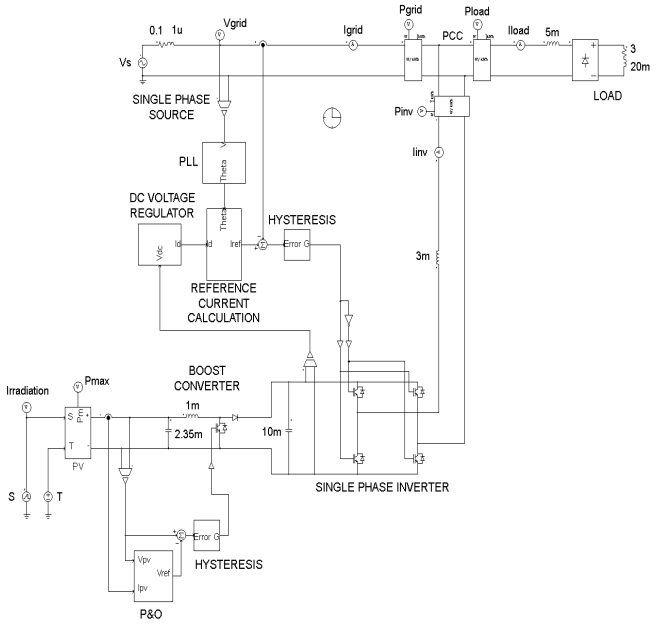

Fig. 10 The PSIM simulation block

A. Power Injection

Fig. 11 and Fig. 12 show the power-voltage and current-voltage curves for the PV array in the PSIM simulation at solar irradiation (S) 250, 500, 750, and 1000 W/m^2 and the temperature (T) at 25°C.

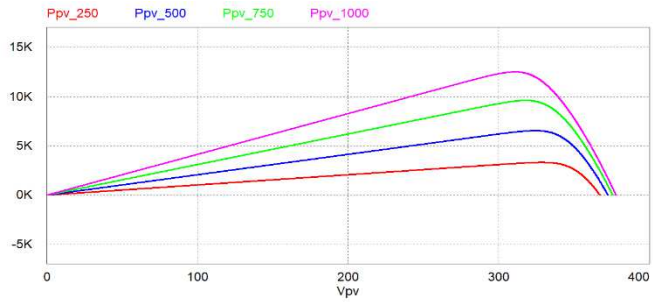

Fig. 11 Power-voltage curve for PV array

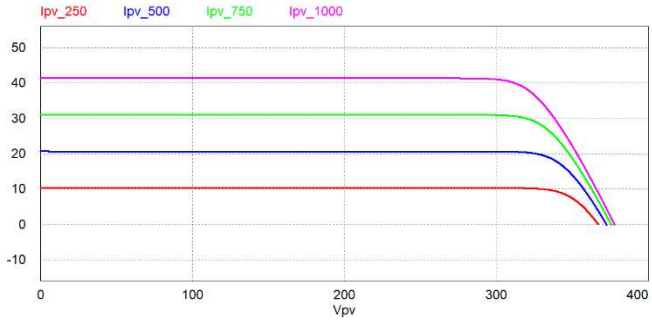

Fig. 12 Current-voltage curve for PV array

From these figures, Table 3 shows the maximum power point for the PV array at irradiation (S) 250, 500, 750, and 1000 W/m^2. The temperature remains constant at 25 °C.

TABLE III
MAXIMUM POWER POINT FOR PV ARRAY (T = 25 °C)

S (W/m^2)	P_m (kW)	V_m (V)	I_m(A)
250	3.3	328.5	10.1
500	6.5	324.2	20.2
750	9.6	317.9	30.2
1000	12.5	310.7	40.3

When the irradiation was 1000 W/m^2, and the temperature was 25°C (STC condition), the simulation results, as shown in Table 3 has been in line with the PV module specifications, as shown in Table 1.

$$V_m = V_{MPP} \, x \, 10 = 31.1 \, x \, 10 = 311 \; V \; (10 \; series)$$

$$I_m = I_{MPP} \, x \, 5 = 8.05 \, x \, 5 = 40.25 \; A \; (5 \; parallel)$$

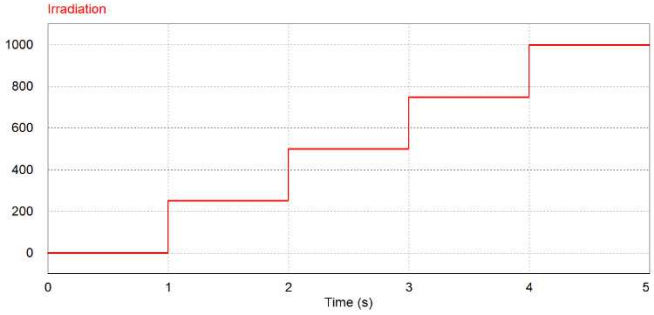

Fig. 13 Irradiation variation (W/m^2)

The simulation was carried out for 5 seconds. Fig. 13 shows the irradiation variation from 0 to 1000 W/m^2 for 5s in increments of 250 W/m^2 per second. The maximum PV power and the power delivered from PV to PCC are shown in Fig. 14. From this figure. It can be shown that the converter can deliver the maximum power generated by the PV. This showed that the boost converter control using the P&O algorithm worked properly.

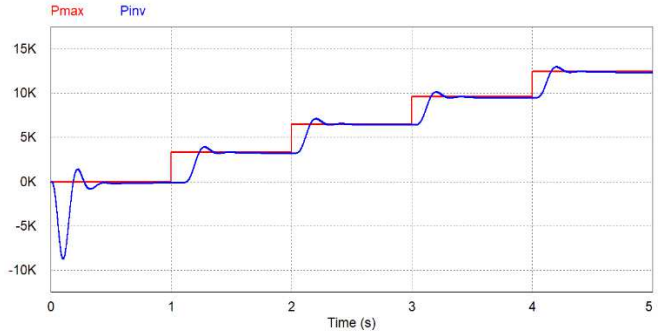

Fig. 14 Power delivery from PV to PCC (Pinv) track maximum power (Pmax)

Fig. 15 shows grid power, inverter power, and load power. It can be seen that the load power was relatively constant, while the grid power and inverter power varied dependent upon the irradiation. The grid delivered power to the load at t = 0-3s ($P_{grid} > 0$) and received power at t = 3-5s ($P_{grid} < 0$). This was because when t=3-5s, PV produced more power than the load power when solar irradiations were 750 W/m^2 and 1000 W/m^2.

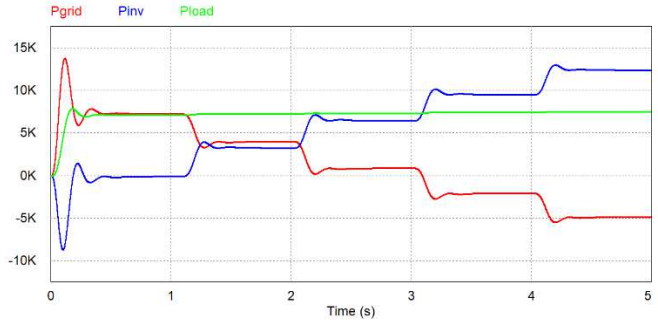

Fig. 15 Grid power (P_{grid}), inverter power (P_{inv}), and load power (P_{load})

Table 4 shows the power flow on the grid, inverter, and load at irradiation of 0 - 1000 W/m^2. It can be seen in Table 4 that MPPT can function properly for maximum power transfer and the power produced by PV (P_{inv}) is close to the maximum power (P_m) as based on Table 3.

TABLE IV
POWER FLOW ON GRID, INVERTER, AND LOAD

S (W/m^2)	P_{grid} (kW)	P_{inv} (kW)	P_{load} (kW)
0	7.2	-0.1	7.1
250	4.0	3.2	7.2
500	0.9	6.4	7.3
750	-0.2	9.5	7.4
1000	-4.9	12.4	7.5

When solar irradiation was 0 W/m^2, the grid provided the entire load of power. At S = 250 W/m^2 and S = 500 W/m^2, P_{grid} and P_{inv} had a positive sign, which meant that the grid and PV simultaneously delivered power to the PCC. While when S = 750 W/m^2 and S = 1000 W/m^2, P_{grid} had a negative sign and P_{inv} had a positive sign – meaning that the grid received power from PV. The additional power was fed back to the grid because PV generated more power than the load power.

B. Power Quality Improvement

To show the performance of the inverter in compensating reactive power and mitigating harmonics, the analysis was carried out for 3 (three) conditions: (a) PV power = 0, (b) PV power < load power, and (c) PV power > load power

1) PV power = 0: This condition was obtained when the solar irradiation was 0 W/m^2. PV did not produce power in this condition, but the grid provided an entire power demand load. However, the inverter still functioned as an active power filter.

Fig. 16 shows the grid voltage and grid current waveforms when irradiation and temperature were at 0 W/m^2 and 25°C for t = 0.9 – 1s, respectively. It showed the grid voltage (V_{grid}) and grid current (I_{grid}) in phase showing the achievement of unity power factor (UPF). It was then proven that the inverter could compensate for load-reactive power demand. Power factor (PF) prior to compensation at 0.71 lag coming to be at 1.0 after compensation.

The profiles for the grid, inverter and load currents are shown in Fig. 17. This figure shows that the load current was not sinusoidal due to nonlinearities load. The THD_i of load current (I_{load}) was 18.3%. The inverter worked properly to compensate for the load current harmonic, so the grid current remained sinusoidal. The THD_i of grid currents (I_{grid}) was reduced to 2.3% after compensation.

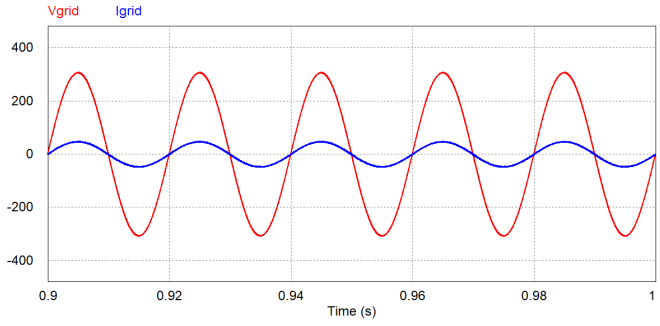

Fig. 16 Waveforms for grid voltage and grid current (S=0 W/m^2 and T=25°C)

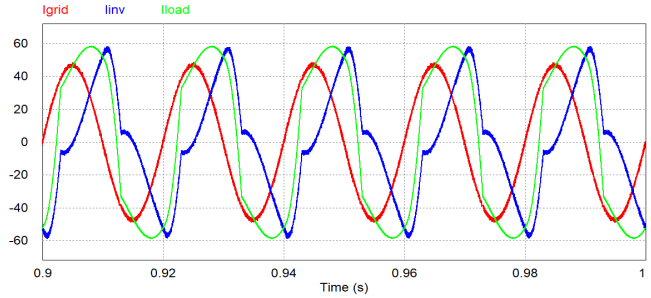

Fig. 17 Waveforms for grid, inverter and load current (S=0 W/m^2 and T=25°C)

2) PV power < load power: Fig. 15 and Table 4 show that when solar irradiation is 250 W/m^2 and 500 W/m^2, PV produces less power than the load demand. The power generated by PV is delivered to the PCC via an inverter. In addition to power transfer, the inverter also functions as an active power filter.

The grid voltage and grid current profiles when irradiation was at 250 W/m^2 and temperature of 25°C are shown in Fig. 18. Grid voltage and grid current were in phase. The inverter could compensate for reactive power well. With the inverter installed, the power factor increased from 0.71 lag to 1.0. In addition, the inverter has also successfully carried out harmonic mitigation. It can be seen from the current profile shown in Fig. 19. Before compensation, the THD$_i$ was 18.3%. After the inverter installed, the THD$_i$ of grid currents (I_{grid}) were reduced to be 4.1%.

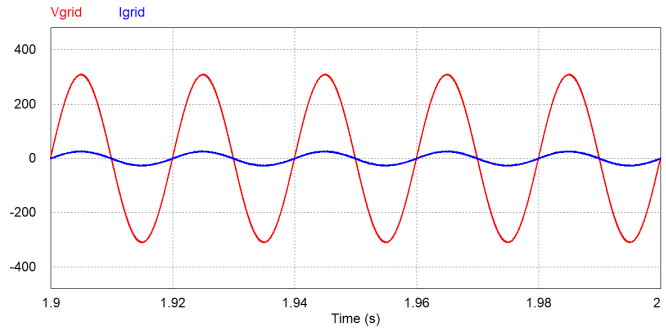

Fig. 18 Waveforms for grid voltage and grid current (S=250 W/m^2 and T=25°C)

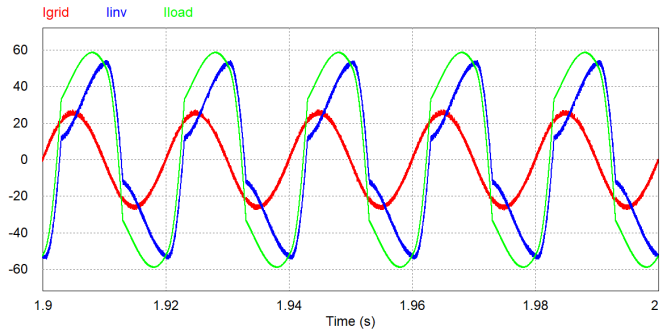

Fig. 19 Waveforms for the grid, inverter, and load current (S=250 W/m^2 and T=25°C)

3) PV power > load power: Fig. 15 and Table 4 show that the power produced by PV was greater than the load power when solar irradiations were at 750 W/m^2 and 1000 W/m^2. The power generated by this PV was supplied to the grid and load.

Fig. 20 shows the profiles of grid voltage and grid current when irradiation was at 1000 W/m^2 and temperature of 25°C. Grid voltage and grid current were 180° out of phase. It means that the inverter delivered the additional generated power to the grid at the unity power factor. In this condition, the inverter can compensate for the reactive power well in which the power factor changed from 0.71 lag to -1.0. Harmonic mitigation was also successfully carried out; THD$_i$ changed from 18.3% to 3.3%. It can be seen in Fig. 21, which shows the profiles for the grid, inverter, and load currents.

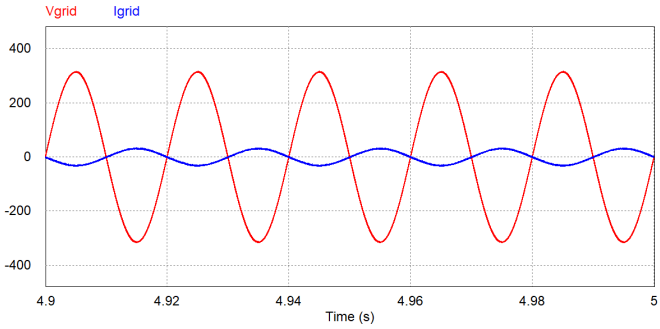

Fig. 20 Waveforms for grid voltage and grid current (S=1000 W/m^2 and T=25°C)

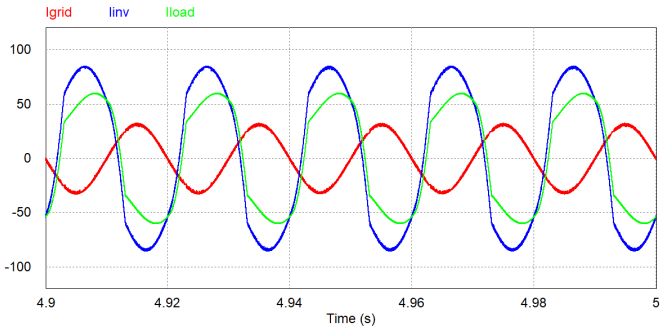

Fig. 21 Waveforms for grid, inverter, and load currents (S=1000 W/m^2 and T=25°C)

Table 5 presents a summary of RMS grid current, power factor, and THD$_i$ after compensation. Here, there were 3 conditions: (a) PV power = 0 (S = 0 W/m^2), (b) PV power < load power (S = 250 W/m^2), and (c) PV power > load power (S = 1000 W/m^2). This table shows that there has been an improvement in the power factor and harmonics.

TABLE V
POWER QUALITY IMPROVEMENT AFTER COMPENSATION

Condition	S (W/m^2)	$I_{grid\text{-}RMS}$ (A)	PF	THDi(%)
$P_{PV} = 0$	0	33.4	1	2.3
$P_{PV} < P_{load}$	250	18.3	1	4.1
$P_{PV} > P_{load}$	1000	22.0	-1	3.3

PF before compensation = 0.71 lag
THD$_i$ before compensation = 18.3%

IV. CONCLUSION

This research has presented the control for an on-grid inverter for PV applications. The single-phase inverter was controlled so that the grid only drew or supplied the active power. This inverter can deliver the maximum power generated by the PV and operate as an Active Power Filter (APF). The PSIM simulation showed that the inverter could work properly. Three goals have been successfully carried out: maximum power transfer, power factor compensation, and reduced harmonic distortion.

The PV can generate the maximum power according to the irradiation (S = 0 - 1000 W/m^2). This showed that the boost converter control using the P&O algorithm worked properly.

When irradiation 0. 250, and 500 W/m^2, the grid and PV supplied the load power demand because the load power demand was more than the PV power. Conversely, if the load power demand was less than the PV power (irradiation 750 W/m^2 and 1000 W/m^2), the grid received this additional power.

Power quality improvement can be achieved for three conditions: (a) PV power = 0, (b) PV power < load power, and (c) PV power > load power. For all these conditions, the grid current is always sinusoidal. When PV power = 0, there is no power generation from PV, so the inverter only functions as an active power filter (harmonic and reactive power compensation). When PV power < load power, PV and grid together supply the load. In this condition, the inverter also functions as an active power filter. The active power will be delivered from the grid to the load at pf = 1. When PV power > load power, the inverter will fulfill the total load power demand. Additional active power will be delivered to the grid at the unity power factor. The results of the work can be used in the design and operation of a single-phase on-grid PV inverter. In the future, we plan to perform experiments in the laboratory for performance validation.

ACKNOWLEDGMENTS

We thank Diponegoro University for supporting this research through the PTUPT research scheme.

REFERENCES

[1] S. Mukhtarov, J. I. Mikayilov, S. Maharramov, J. Aliyev, and E. Suleymanov, "Higher Oil Prices, Are they Good or Bad for Renewable Energy Consumption: The Case of Iran?," *Renew. Energy*, 2022, doi: 10.1016/j.renene.2021.12.135.

[2] F. Zhang, X. Wang, M. Wu, X. Hou, C. Han, and Z. Liu, "Optimization design of uncertain parameters for improving the stability of photovoltaic system," *J. Power Sources*, vol. 521, no. December 2021, p. 230959, 2022, doi: 10.1016/j.jpowsour.2021.230959.

[3] J. Gong, D. Li, T. Wang, W. Pan, and X. Ding, "A comprehensive review of improving power quality using active power filters," *Electr. Power Syst. Res.*, vol. 199, no. April, p. 107389, 2021, doi: 10.1016/j.epsr.2021.107389.

[4] M. Malik and P. R. Sharma, "A scheme for reduction in harmonics and establish the stability of hybrid system connected in grid," *Ain Shams Eng. J.*, vol. 11, no. 4, pp. 1123–1130, 2020, doi: 10.1016/j.asej.2020.02.013.

[5] R. B. N., M. Venu Gopala Rao, and R. Srinivasa Rao, "Battery Energy Integrated Active Power Filter for Harmonic Compensation and Active Power Injection," *Sustain. Comput. Informatics Syst.*, p. 100664, 2022, doi: 10.1016/j.suscom.2022.100664.

[6] R. Kumar, "Fuzzy particle swarm optimization control algorithm implementation in photovoltaic integrated shunt active power filter for power quality improvement using hardware-in-the-loop," *Sustain. Energy Technol. Assessments*, vol. 50, no. May 2021, p. 101820, 2022, doi: 10.1016/j.seta.2021.101820.

[7] S. Echalih, A. Abouloifa, I. Lachkar, J. M. Guerrero, Z. Hekss, and F. Giri, "Hybrid automaton-fuzzy control of single phase dual buck half bridge shunt active power filter for shoot through elimination and power quality improvement," *Int. J. Electr. Power Energy Syst.*, vol. 131, no. March 2020, p. 106986, 2021, doi: 10.1016/j.ijepes.2021.106986.

[8] Z. Li, L. Wang, Y. Wang, and G. Li, "Harmonic detection method based on adaptive noise cancellation and its application in photovoltaic - active power filter system," *Electr. Power Syst. Res.*, vol. 184, no. March, p. 106308, 2020, doi: 10.1016/j.epsr.2020.106308.

[9] J. A. Cortajarena, O. Barambones, P. Alkorta, and J. Cortajarena, "Sliding mode control of an active power filter with photovoltaic maximum power tracking," *Electr. Power Energy Syst.*, vol. 110, no. March, pp. 747–758, 2019, doi: 10.1016/j.ijepes.2019.03.070.

[10] M. Aourir *et al.*, "Nonlinear control of multicellular single stage grid connected photovoltaic systems with shunt active power filtering capability," *IFAC-PapersOnLine*, vol. 53, no. 2, pp. 12853–12858, 2020, doi: 10.1016/j.ifacol.2020.12.2091.

[11] S. Ouchen, H. Steinhart, M. Benbouzid, and F. Blaabjerg, "Robust DPC-SVM control strategy for shunt active power filter based on H∞ regulators," *Electr. Power Energy Syst.*, vol. 117, no. May 2019, p. 105699, 2020, doi: 10.1016/j.ijepes.2019.105699.

[12] Z. Hekss *et al.*, "Hybrid automaton control of three phase reduced switch shunt active power filter connected photovoltaic system," *IFAC-PapersOnLine*, vol. 53, no. 2, pp. 12847–12852, 2020, doi: 10.1016/j.ifacol.2020.12.1986.

[13] E. Samavati and H. R. Mohammadi, "Simultaneous voltage and current harmonics compensation in islanded/grid-connected microgrids using virtual impedance concept," *Sustain. Energy, Grids Networks*, vol. 20, p. 100258, 2019, doi: 10.1016/j.segan.2019.100258.

[14] F. Deng, A. Petucco, P. Mattavelli, and X. Zhang, "An enhanced current sharing strategy for islanded ac microgrids based on adaptive virtual impedance regulation," *Int. J. Electr. Power Energy Syst.*, vol. 134, no. July 2021, p. 107402, 2022, doi: 10.1016/j.ijepes.2021.107402.

[15] A. Sahli, F. Krim, A. Laib, and B. Talbi, "Model predictive control for single phase active power filter using modified packed U-cell (MPUC5) converter," *Electr. Power Syst. Res.*, vol. 180, no. December 2019, p. 106139, 2020, doi: 10.1016/j.epsr.2019.106139.

[16] S. Asapu and V. R, "Modified hysteresis current control of multilevel converter for grid connected battery storage system," *Mater. Today Proc.*, no. xxxx, 2021, doi: 10.1016/j.matpr.2021.07.290.

[17] A. Azzam-Jai and M. Ouassaid, "Photovoltaic Interfaced Shunt Active Power Filter Under Online-Varying Parameters Based On Fuzzy Logic Controller And Adaptive Hysteresis Band Current Controller," in *3rd International Conference on Intelligent Computing in Data Sciences, ICDS*, 2019, pp. 1–7, doi: 10.1109/ICDS47004.2019.8942282.

[18] I. Setiawan, A. Priyadi, and M. H. Purnomo, "Control Strategy Based on Associative Memory Networks for a Grid-Side Converter in On-Grid Renewable Generation Systems Under Generalized Unbalanced Grid Voltage Conditions," *Int. Rev. Electr. Eng.*, vol. 11, pp. 171–182, 2016.

[19] P. S. Sanjan, N. G. Yamini, and N. Gowtham, "Performance Comparison of Single-Phase SAPF Using PQ Theory and SRF Theory," *International Conf. Emerg. Technol.*, p. 9154126, 2020, doi: 10.1109/INCET49848.2020.9154126.

[20] S. M. Bagi, F. N. Kudchi, and S. Bagewadi, "Power Quality Improvement using a Shunt Active Power Filter for Grid Connected Photovoltaic Generation System," in *Proceedings of B-HTC 2020 - 1st IEEE Bangalore Humanitarian Technology Conference*, 2020, pp. 1–4, doi: 10.1109/B-HTC50970.2020.9298001.

[21] W. Choi and B. Sarlioglu, "Comparative Analysis on Performance of Power Quality Improvement of Grid-Connected Inverters," *EEE Energy Convers. Congr. Expo.*, pp. 4281–4286, 2019, doi: 10.1109/ECCE.2019.8912488.

[22] W. Choi, K. Jung, and B. Sarlioglu, "Power Control of Hybrid Grid-Connected Inverter to Improve Power Quality," in *ECCE 2020 - IEEE Energy Conversion Congress and Exposition*, 2020, pp. 3741–3745, doi: 10.1109/ECCE44975.2020.9235627.

[23] N. Moharana, D. Dash, and S. K. Dalai, "Power Quality Improvement in PVGrid System," 2021, pp. 1–5, doi: 10.1109/apsit52773.2021.9641469.